Understanding Ligand-Exchange Reactions on Thiolate-Protected Gold Clusters by Probing Isomer Distributions Using Reversed-Phase High-Performance Liquid Chromatography

Yoshiki Niihori,[†] Yoshihiro Kikuchi,[†] Ayano Kato,[†] Miku Matsuzaki,[†] and Yuichi Negishi[*,†,‡,§]

[†]Department of Applied Chemistry, Faculty of Science, Tokyo University of Science, 1-3 Kagurazaka, Shinjuku-ku, Tokyo 162-8601, Japan, [‡]Photocatalysis International Research Center, Tokyo University of Science, 2641 Yamazaki, Noda, Chiba 278-8510, Japan, and [§]Department of Materials Molecular Science, Institute for Molecular Science, Myodaiji, Okazaki, Aichi 444-8585, Japan

ABSTRACT Thiolate-protected gold clusters ($Au_n(SR)_m$) have attracted considerable attention as functional nanomaterials in a wide range of fields. A ligand-exchange reaction has long been used to functionalize these clusters. In this study, we separated products from a ligand-exchange reaction of phenylethanethiolate-protected $Au_{24}Pd$ clusters ($Au_{24}Pd(SC_2H_4Ph)_{18}$), in which $Au_{25}(SR)_{18}$ is doped with palladium, into each coordination isomer with high resolution by reversed-phase high-performance liquid chromatography. This success has enabled isomer distributions of the products to be quantitatively evaluated. We evaluated quantitatively the isomer distributions of products obtained by the reaction of $Au_{24}Pd(SC_2H_4Ph)_{18}$ with thiol, disulfide, or diselenide. The results revealed that the exchange reaction starts to occur preferentially at thiolates that are bound directly to the metal core (thiolates of a core site) in all reactions. Further study on the isomer-separated $Au_{24}Pd(SC_2H_4Ph)_{17}(SC_{12}H_{25})$ revealed that clusters vary the coordination isomer distribution in solution by the ligand-exchange reaction between clusters and that control of the coordination isomer distribution of the starting clusters enables control of the coordination isomer distribution of the products generated by ligand-exchange reactions between clusters. $Au_{24}Pd(SC_2H_4Ph)_{18}$ used in this study has a similar framework structure to $Au_{25}(SR)_{18}$, which is one of the most studied compounds in the $Au_n(SR)_m$ clusters. Knowledge gained in this study is expected to enable further understanding of ligand-exchange reactions on $Au_{25}(SR)_{18}$ and other $Au_n(SR)_m$ clusters.

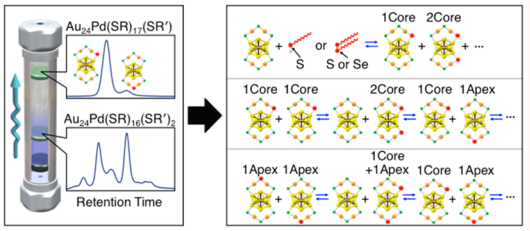

KEYWORDS: thiolate-protected gold clusters · ligand-exchange reaction · reversed-phase high-performance liquid chromatography · coordination isomer · isomer distribution

Advances in nanotechnology have encouraged the creation of stable, highly functionalized nanomaterials. Thiolate-protected gold clusters ($Au_n(SR)_m$)[1−4] exhibit a high stability in solution and in the solid state compared with other metal clusters. In addition, they can be synthesized precisely at the atomic level[5−12] and therefore are well understood by experimental and theoretical studies.[13−18] Furthermore, these clusters exhibit size-specific physical or chemical properties, such as photoluminescence,[1,3,5,6,19,20] redox behavior,[3,21] and catalytic activity,[22−26] which are not observed in bulk gold. Consequently, $Au_n(SR)_m$ clusters are attracting considerable attention in a wide range of fields from nanoscience to nanotechnology.

The ligand-exchange reaction has long been used to functionalize these $Au_n(SR)_m$ clusters. This method enables a new ligand to be introduced to the $Au_n(SR)_m$ clusters and imparts new functionality.[27,28] Furthermore, the method allows $Au_n(SR)_m$ clusters with unique chemical compositions to be synthesized with high yield. For example, when $Au_{38}(SC_2H_4Ph)_{24}$ and 4-*tert*-butylbenzenethiol (TBBT) react in solution, a distortion

* Address correspondence to negishi@rs.kagu.tus.ac.jp.

Received for review June 6, 2015 and accepted July 13, 2015.

Published online July 13, 2015
10.1021/acsnano.5b03435

of the metal core is induced in addition to the ligand exchange, which leads to the formation of $Au_{36}(TBBT)_{24}$ with a yield of ~90%.[29,30] $Au_{28}(TBBT)_{20}$ and $Au_{133}(TBBT)_{52}$ have also been synthesized similarly from $Au_{25}(SC_2H_4Ph)_{18}$ and $Au_{144}(SC_2H_4Ph)_{60}$, respectively.[31−33] Therefore, the ligand-exchange reaction is an extremely useful method to functionalize clusters and synthesize unique clusters.

Many studies have been carried out on ligand-exchange reaction mechanisms. The pioneering work of Murray and co-workers used mainly nuclear magnetic resonance and mass spectrometry. Their research provided extensive information on the rates of ligand-exchange reactions[34,35] and the chemical composition distributions of the products.[35−37] Ackerson and co-workers conducted single-crystal X-ray structure analysis of $Au_{25}(SC_2H_4Ph)_{16}(p\text{-BBT})_2$ and $Au_{102}(p\text{-MBA})_{40}$ (*p*-BBT = *p*-bromobenzenethiol, *p*-MBA = *p*-mercaptobenzoic acid).[38,39] Their work clarified the geometric structures of the products. On the basis of the obtained geometric structures, Ackerson and co-workers proposed the presence of sites at which reactions were more likely to take place. However, as Ackerson and co-workers suggested, the obtained geometric structure may be only one of multiple products present.[39] Indeed, Bürgi and co-workers showed by high-performance liquid chromatography (HPLC) with a chiral column that multiple coordination isomers of $Au_{38}(SC_2H_4Ph)_{23}$(PCP-4-S) could be produced by the reaction between $Au_{38}(SC_2H_4Ph)_{24}$ and [2.2]paracyclophane-4-thiol (PCP-4-SH).[40] The variety of the reaction sites has also been predicted in the early stage studies by Murray and co-workers.[37] Thus, distributions of the generated coordination isomers should be evaluated quantitatively to increase the understanding of the mechanism in ligand-exchange reactions.

In this study, we have achieved quantitative determinations of the coordination isomer distributions of products obtained by ligand-exchange reactions using reversed-phase (RP)-HPLC. RP-HPLC is a familiar separation or analytical method that is used in the study of $Au_n(SR)_m$ clusters.[11,41−44] We have recently found that products of ligand-exchange reactions can be separated by RP-HPLC combined with mobile phase substitution with high resolution depending on ligand combinations.[45,46] In this study, we found for $Au_{24}Pd(SC_2H_4Ph)_{18}$ (refs 43, 47−49) ($Au_{25}(SR)_{18}$ (refs 50−52) doped with palladium), that even the coordination isomers could be separated with a high resolution when an appropriate solvent was used as the mobile phase. We have evaluated quantitatively the isomer distributions of the products obtained by ligand-exchange reactions between $Au_{24}Pd(SC_2H_4Ph)_{18}$ and thiol, disulfide, or diselenide using this high-resolution separation method. We have found that there is a significant bias in the isomer distributions of the products, and in all of the aforementioned reactions, exchange reactions start to occur preferentially at thiolates that are bound directly to the metal core (thiolates of core site). We further studied the temporal evolution of isomer-separated $Au_{24}Pd(SC_2H_4Ph)_{17}(SC_{12}H_{25})$ using our high-resolution separation method. The results provide insights into how isomer distributions arise in the clusters and how coordination isomer distribution in the clusters can be controlled.

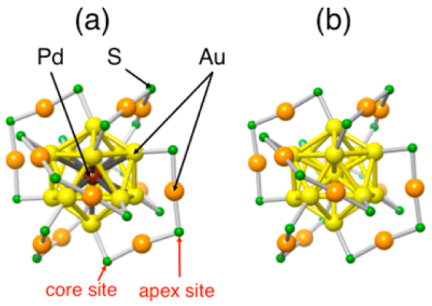

Figure 1. Geometrical structures determined for (a) $Au_{24}Pd(SR)_{18}$ (refs 43, 48, and 49) and (b) $Au_{25}(SR)_{18}$ (refs 50 and 51). The R groups are omitted for simplicity. Two sites of sulfur (S) discussed in this manuscript are explained in (a).

RESULTS AND DISCUSSION

In this study, we used $Au_{24}Pd(SC_2H_4Ph)_{18}$ (Figure 1(a) and S1) as the metal cluster for the following reasons. (i) $Au_{24}Pd(SR)_{18}$ has a geometric structure in which Au at the center of $Au_{25}(SR)_{18}$ (Figure 1(b)) is substituted by Pd (Figure S2). Therefore, $Au_{24}Pd(SR)_{18}$ has a similar framework structure to $Au_{25}(SR)_{18}$, which is one of the most extensively studied compounds of the $Au_n(SR)_m$ clusters.[43,47−49] (ii) The ligand-exchange reaction between two $Au_{24}Pd(SR)_{18}$ molecules does not occur as readily as that between two $Au_{25}(SR)_{18}$ molecules.[53] Therefore, in experiments with $Au_{24}Pd(SR)_{18}$, ligand-exchange reactions between the generated coordination isomers could be suppressed and isomer distributions of the products can be determined more reliably.

High-Resolution Product Separation. In this section, we describe the product obtained from the reaction between $Au_{24}Pd(SC_2H_4Ph)_{18}$ (Figure 1(a)) and $C_{12}H_{25}SH$. The ligand-exchange reaction was induced by stirring $Au_{24}Pd(SC_2H_4Ph)_{18}$ and $C_{12}H_{25}SH$ (concentration ratio of 1:50) in dichloromethane for 4 min. Figure 2 shows the matrix-assisted laser desorption/ionization (MALDI) mass spectrum of the products. The mass spectrum exhibits peaks attributable to $Au_{24}Pd(SC_2H_4Ph)_{18-n}(SC_{12}H_{25})_n$ (n = 0−7). This indicates that the ligand-exchange reaction took place under our experimental conditions.[36]

The obtained products were separated by HPLC using an octadecylsilyl column (Figure S3(a)). All products were first adsorbed on the stationary phase by injecting a suspension of clusters into the column in which a solvent incapable of dissolving the clusters (adsorption solvent) was used as mobile phase. Then,

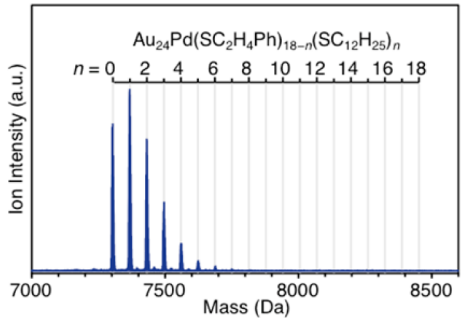

Figure 2. Negative-ion MALDI mass spectrum of the product obtained from the reaction between $Au_{24}Pd(SC_2H_4Ph)_{18}$ and $C_{12}H_{25}SH$ in dichloromethane at $[C_{12}H_{25}SH]/[Au_{24}Pd(SC_2H_4Ph)_{18}] = 50$.

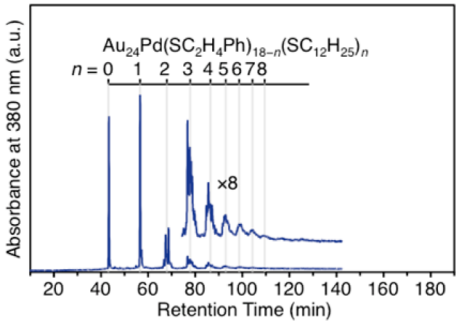

Figure 3. Chromatogram of product obtained from the reaction between $Au_{24}Pd(SC_2H_4Ph)_{18}$ and $C_{12}H_{25}SH$ in dichloromethane at $[C_{12}H_{25}SH]/[Au_{24}Pd(SC_2H_4Ph)_{18}] = 50$.

the products were eluted from the stationary phase in order of cluster surface polarity (Figure S3(b)) by gradually introducing a solvent capable of dissolving the clusters (elution solvent) into the mobile phase using a linear gradient program (Figure S4). Our previous studies revealed that $Au_{24}Pd(SC_2H_4Ph)_{18-n}(SC_{12}H_{25})_n$ could be separated with high resolution depending on the ligand combinations by this method. In those studies, methanol and tetrahydrofuran (THF) were used as the adsorption and elution solvents, respectively.[45,46] Under these experimental conditions, the mobile phase polarity is higher than that of the stationary phase (Figure S3(a)); thus, the clusters are separated in the reversed-phase mode. In this study, acetonitrile and acetone were used as the adsorption and elution solvents instead of methanol and THF, respectively (Table S1). As a result, a peak attributed to a cluster with a single chemical composition was separated into multiple peaks (Figures S5 and S6).

Figure 3 shows the chromatogram of the obtained products, which features a peak distribution similar to that in the MALDI mass spectrum (Figure S7). This demonstrates that $Au_{24}Pd(SC_2H_4Ph)_{18-n}(SC_{12}H_{25})_n$ ($n = 0-7$) was separated with high resolution depending on the ligand combinations under our experimental conditions. Figure 4 shows an enlarged view of a peak group attributed to $Au_{24}Pd(SC_2H_4Ph)_{18-n}(SC_{12}H_{25})_n$ ($n = 0-5$). Only one peak exists for $Au_{24}Pd(SC_2H_4Ph)_{18}$ (Figure 4(a)). Two peaks exist for $Au_{24}Pd(SC_2H_4Ph)_{17}(SC_{12}H_{25})$ (Figure 4(b)) and more peaks are visible for $Au_{24}Pd(SC_2H_4Ph)_{18-n}(SC_{12}H_{25})_n$ ($n = 2-5$) (Figure 4(c–f)). In the MALDI mass spectrum of each fraction in Figure 4, only a peak attributable to the single chemical composition of $Au_{24}Pd(SC_2H_4Ph)_{18-n}(SC_{12}H_{25})_n$ ($n = 0-5$) was observed (Figure 5), which demonstrates that only the clusters of the single chemical composition were contained in the fractions of Figure 4(a–f). These results indicate that each coordination isomer of $Au_{24}Pd(SC_2H_4Ph)_{18-n}(SC_{12}H_{25})_n$ ($n = 0-5$) was separated with high resolution under our experimental conditions. Acetonitrile (0.369 mPa s at 25 °C) and acetone (0.306 mPa s at 25 °C) are solvents with a lower viscosity than methanol (0.544 mPa s at 25 °C) and THF (0.456 mPa s at 25 °C), respectively.[54] It is presumed that the coordination isomers were separated with high resolution under these experimental conditions (Figure S8), because the variations in cluster elution times from the stationary phase are suppressed or the interaction number between the stationary phase and clusters (the theoretical plate number) after the elution is increased by a decrease in the viscosities of the adsorption and elution solvents.[55] Several other factors may also contribute to the higher resolution. Regardless of the main cause, the above result indicates that when appropriate experimental conditions are chosen, the products can be separated into each coordination isomer with high resolution by RP-HPLC, and quantitative evaluation of the coordination isomers by RP-HPLC is then possible.

Reaction Mechanism: Reaction with Thiol. On the basis of the separated peaks, we considered the exchange site in the ligand-exchange reaction between $Au_{24}Pd(SC_2H_4Ph)_{18}$ and $C_{12}H_{25}SH$. We consider first the initial ligand-exchange site. As shown in Figure 4(b), the chromatogram of $Au_{24}Pd(SC_2H_4Ph)_{17}(SC_{12}H_{25})$ exhibited two peaks with retention times of 56.58 and 57.20 min. Their area ratio was calculated to be 12:0.9 by curve-fitting of these peaks (Figure 4(b)). This result indicates that the isomer distribution of the $Au_{24}Pd(SC_2H_4Ph)_{17}(SC_{12}H_{25})$ products was strongly biased.

To determine the species responsible for the observed peaks, the obtained samples were left in acetone at room temperature and variations in the relative intensities of the two peaks were studied. Figure 6(a) shows a temporal evolution of the chromatogram of $Au_{24}Pd(SC_2H_4Ph)_{17}(SC_{12}H_{25})$. The relative intensity of the peak at 57.20 min increased with time. This indicates that the difference in thermodynamic stability between the two coordination isomers was not significant. Note that a similar change in the distribution of the coordination isomers has also been observed by Bürgi and co-workers for the reaction between $Au_{38}(SR)_{24}$ and PCP-4-SH.[40] When the area ratio approached

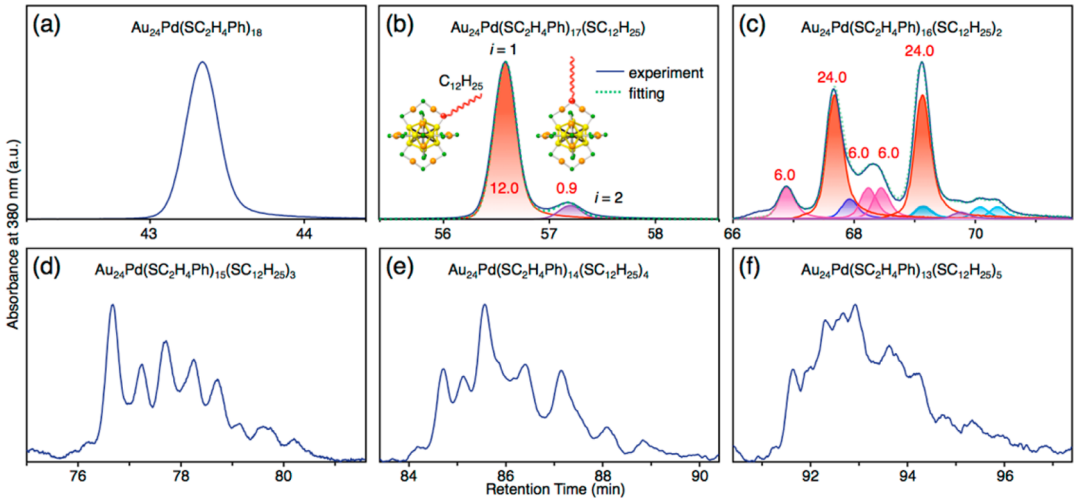

Figure 4. Expanded chromatograms for regions of (a) $Au_{24}Pd(SC_2H_4Ph)_{18}$, (b) $Au_{24}Pd(SC_2H_4Ph)_{17}(SC_{12}H_{25})$, (c) $Au_{24}Pd(SC_2H_4Ph)_{16}(SC_{12}H_{25})_2$, (d) $Au_{24}Pd(SC_2H_4Ph)_{15}(SC_{12}H_{25})_3$, (e) $Au_{24}Pd(SC_2H_4Ph)_{14}(SC_{12}H_{25})_4$, and (f) $Au_{24}Pd(SC_2H_4Ph)_{13}(SC_{12}H_{25})_5$. The fitting results are also shown in (b,c). In these fittings, the peak structure used for fitting is based on the peak structure of $Au_{24}Pd(SC_2H_4Ph)_{18}$ of (a), because the peak structure in the chromatogram does not show a symmetrical curve (see (a)).

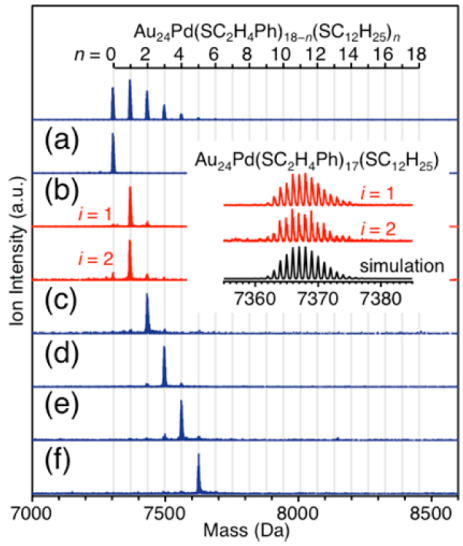

Figure 5. Negative-ion MALDI mass spectra of fractions shown in Figure 4(a–f). (a–f) show the mass spectra of the fractions shown in Figure 4(a–f), respectively. Two isomers of isomer index i = 1, 2 (Figures 4(b) and 7(a,c)), which were separated by RP-HPLC, are shown for the fraction of Figure 4(b). In each mass spectrum of (a–f), a peak attributed to a single $Au_{24}Pd(SC_2H_4Ph)_{18-n}(SC_{12}H_{25})_n$ (n = 0–5) was mainly observed. The minor peaks observed in (b–f) are attributed to clusters generated by the reaction between two $Au_{24}Pd(SC_2H_4Ph)_{18-n}(SC_{12}H_{25})_n$ while drying the sample for mass measurements (see Figure 9).

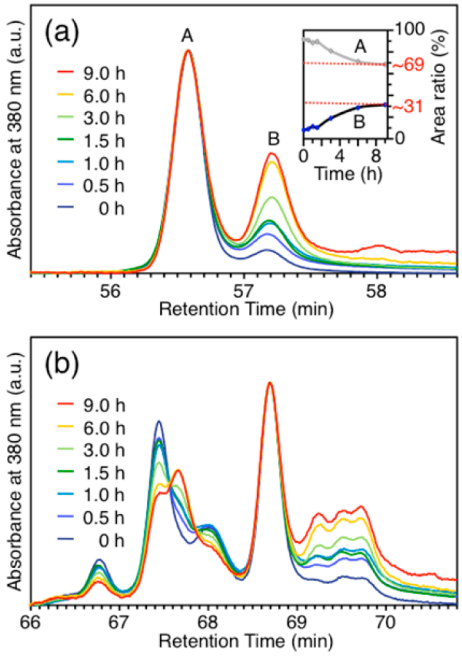

Figure 6. Time dependence of chromatograms of regions of (a) $Au_{24}Pd(SC_2H_4Ph)_{17}(SC_{12}H_{25})$ and (b) $Au_{24}Pd(SC_2H_4Ph)_{16}(SC_{12}H_{25})_2$. In (a,b), all the chromatograms are normalized with the strongest peaks. In (a), the inset shows the time dependence of the area ratio of peaks A and B.

2:1, no further change was observed in their relative intensities (Figure 6(a)). $Au_{24}Pd(SR)_{18}$ used in this study has a geometric structure in which six [-S(R)-Au-S(R)-Au-S(R)-] staples surround the $Au_{12}Pd$ metal core (Figure 1(a)). Two types of SR units exist in such a geometric structure, namely, SR that is bound directly to the metal core (core site) and SR that is positioned at the center of the staple (apex site). The numbers of each type of SR unit are 12 and 6, respectively, which gives a ratio of 2:1 (Figure 7(a,c)). These results imply that peaks with retention times of 56.58 and 57.20 min could be attributed to isomers exchanged at the core and apex sites, respectively (Figure 4(b)). In the isomer with $SC_{12}H_{25}$ at a core site (core-site isomer), the $C_{12}H_{25}$ chain, which interacts more strongly with the stationary phase than C_2H_4Ph, is expected to exist closer to the interior (Figure S9) than in the isomer with $SC_{12}H_{25}$ at an apex site (apex-site isomer). The core-site isomer may interact less efficiently with the stationary phase

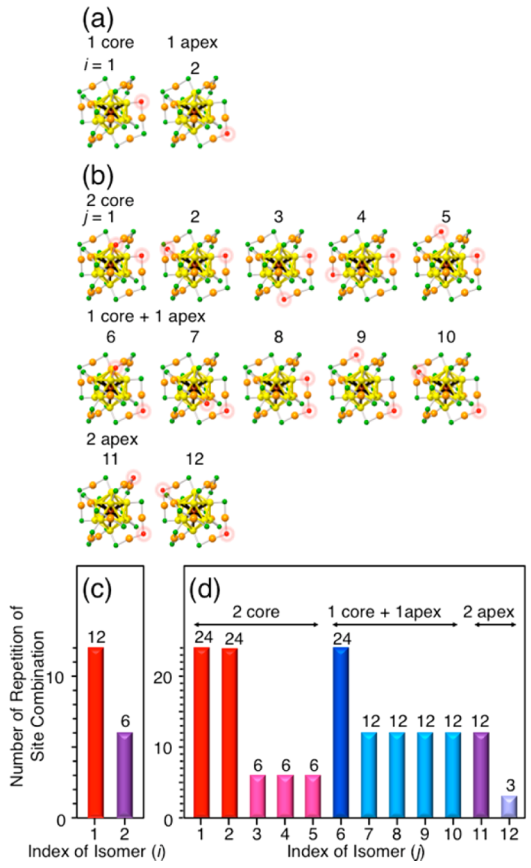

Figure 7. Coordination isomers considered for (a) in $Au_{24}Pd(SC_2H_4Ph)_{17}(SC_{12}H_{25})$ with isomer index, *i*, and (b) $Au_{24}Pd(SC_2H_4Ph)_{16}(SC_{12}H_{25})_2$ with isomer index, *j*. (c) The number of repetitions of site combinations for each isomer with isomer index, *i* and *j*, are summarized in (c) or (d), respectively (Table S2).

because of this difference and thereby elute earlier than the apex-site isomer (Figure S10).

Thus, the $Au_{24}Pd(SC_2H_4Ph)_{17}(SC_{12}H_{25})$ products obtained immediately after the reaction are comprised mainly of core-site isomer. This demonstrates that the first ligand-exchange reaction occurs preferentially at the thiolate of a core site.

Next, we consider the second ligand-exchange site. As shown in Figure 4(c), the chromatogram of $Au_{24}Pd(SC_2H_4Ph)_{16}(SC_{12}H_{25})_2$ shows a larger number of peaks compared with that of $Au_{24}Pd(SC_2H_4Ph)_{17}(SC_{12}H_{25})$. This indicates that there were a large number of coordination isomers in the $Au_{24}Pd(SC_2H_4Ph)_{16}(SC_{12}H_{25})_2$ products. Twelve coordination isomer structures can be considered for $Au_{24}Pd(SC_2H_4Ph)_{16}(SC_{12}H_{25})_2$ (Figure 7(b)). However, fewer than 12 peaks are visible in Figure 4(c). Furthermore, when $Au_{24}Pd(SC_2H_4Ph)_{16}(SC_{12}H_{25})_2$ was left in acetone, the chromatogram shape changed gradually (Figure 6(b)), similar to $Au_{24}Pd(SC_2H_4Ph)_{17}(SC_{12}H_{25})$. These results imply that not all possible coordination isomers were present in the $Au_{24}Pd(SC_2H_4Ph)_{16}(SC_{12}H_{25})_2$ products obtained immediately after the reaction. On the basis of isomer structure of $Au_{24}Pd(SC_2H_4Ph)_{17}(SC_{12}H_{25})$, it is likely that the coordination isomers exchanged at the core sites were present mainly in the $Au_{24}Pd(SC_2H_4Ph)_{16}(SC_{12}H_{25})_2$ products. In the coordination isomers shown in Figure 7(b), five isomers have two $SC_{12}H_{25}$ moieties positioned at core sites (isomer index $j = 1-5$), and 24, 24, 6, 6, and 6 site combinations exist for these five coordination isomers, respectively (Figure 7(d) and Table S2). The main peaks shown in Figure 4(c) could be curve-fitted with such isomers (Figure S11). Our tentative assignments on the $Au_{24}Pd(SC_2H_4Ph)_{16}(SC_{12}H_{25})_2$ peaks (Figure S12 and Table S3) imply that isomers with two $SC_{12}H_{25}$ at the core sites (isomer index $j = 1-5$) are included with a ratio of 81.7% in $Au_{24}Pd(SC_2H_4Ph)_{16}(SC_{12}H_{25})_2$ obtained immediately after the reaction (Figure S11). As shown in Figure 4(b), the initial exchange occurs at a core site with a possibility of 93.0%. These results imply that the second $SC_{12}H_{25}$ moieties are introduced into the remaining core site of $Au_{24}Pd(SC_2H_4Ph)_{17}(SC_{12}H_{25})$ of the core-site isomer with a possibility of 87.7% (Figure S11). Thus, the second exchange still occurs preferentially at the core site, although the priority is slightly less at the second exchange (87.7%) than the initial exchange (93.0%).

Thus, on the basis of a quantitative evaluation of the coordination isomers by RP-HPLC, it was demonstrated that the ligand-exchange reaction starts to occur preferentially at thiolate bound at core sites in the reaction between $Au_{24}Pd(SC_2H_4Ph)_{18}$ and $C_{12}H_{25}SH$. We performed similar experiments while changing the reaction medium from dichloromethane to toluene or acetone. As a result, products exhibited similar chromatograms regardless of the solvent (Figure S13(a,b)). A similar result was also obtained without solvent (Figure S14(a,b)). We conducted similar experiments using other alkanethiols ($R = C_xH_{2x+1}$; $x = 8$, 10, or 14) in place of $C_{12}H_{25}SH$; however, a similar interpretation was obtained from the chromatograms (Figure S15(a,b)). These results imply that the reaction mechanism described above is the main mechanism under many experimental conditions. The results obtained in this work are consistent with the interpretation of the reaction of $Au_{25}(SC_2H_4Ph)_{18}$ with *p*-BBT obtained by Ackerson and co-workers based on single-crystal X-ray structure.[39]

Häkkinen and co-workers performed density functional theory calculations on the ligand-exchange reaction between $Au_{102}(SH)_{44}$ and CH_3SH, and proposed that such a reaction involves initial nucleophilic attack of the S of CH_3SH on the Au of an [-S(H)-Au-S(H)-] staple in $Au_{102}(SH)_{44}$.[38] The H of the SH then bonds to S in the staple, and allows the reaction to proceed. Also, $Au_{24}Pd(SC_2H_4Ph)_{18}$ has staples on its surface (Figure 1(a)). Thus, it can be considered that the reaction starts with a nucleophilic attack of the thiol on Au of the staple, even in the present system (Scheme S1). However, in contrast to $Au_{102}(SH)_{44}$, the

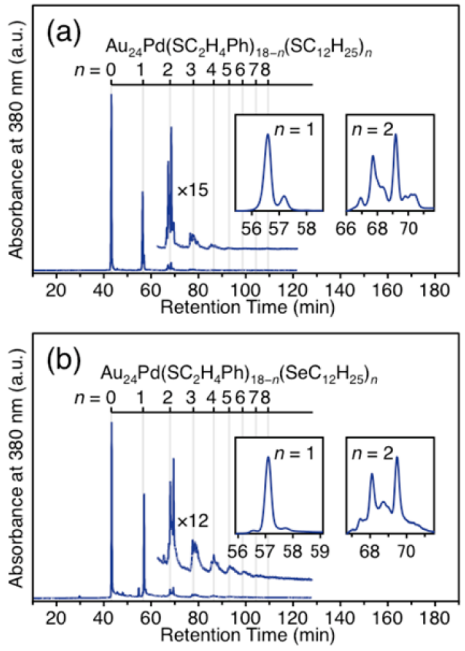

Figure 8. Chromatogram of product obtained by the reaction between (a) $Au_{24}Pd(SC_2H_4Ph)_{18}$ and $(C_{12}H_{25}S)_2$ and (b) $Au_{24}Pd(SC_2H_4Ph)_{18}$ and $(C_{12}H_{25}Se)_2$. These reactions were conducted in dichloromethane at $[(C_{12}H_{25}S)_2]/[Au_{24}Pd(SC_2H_4Ph)_{18}] = 50$ and $[(C_{12}H_{25}Se)_2]/[Au_{24}Pd(SC_2H_4Ph)_{18}] = 10$, respectively.

staples of the present system include two different S atoms that can be attacked by H of the thiol bound to Au; one in a core site, and the other in an apex site (Figure 1(a)). Our results imply that the attack of H of a thiol on S occurs preferentially at the S of a core site on the [-S(R)-Au-S(R)-Au-S(R)-] (R = C_2H_4Ph) staples (Scheme S1).

Reaction Mechanism: Reaction with Disulfide or Diselenide. We have also studied the ligand-exchange reactions of $Au_{24}Pd(SC_2H_4Ph)_{18}$ with other molecules by this method. Figure 8(a) shows a chromatogram of the products obtained by reaction between $Au_{24}Pd(SC_2H_4Ph)_{18}$ and $(C_{12}H_{25}S)_2$ (Figure S16). $Au_{24}Pd(SC_2H_4Ph)_{17}(SC_{12}H_{25})$ exhibited a chromatogram similar to that of the products obtained by the reaction between $Au_{24}Pd(SC_2H_4Ph)_{18}$ and $C_{12}H_{25}SH$ (Figure 4(b)). In the chromatogram of $Au_{24}Pd(SC_2H_4Ph)_{17}(SC_{12}H_{25})$, two peaks attributed to the isomers were estimated to be 12:1.8 through curve-fitting (Figure 8(a)). $Au_{24}Pd(SC_2H_4Ph)_{16}(SC_{12}H_{25})_2$ also exhibited a chromatogram similar to that of Figure 4(c). These results indicate that the exchange reaction occurs preferentially at the core site even if the reactant is not a thiol ($C_{12}H_{25}SH$) but a disulfide ($(C_{12}H_{25}S)_2$). Similar results were also obtained for the reaction between $Au_{24}Pd(SC_2H_4Ph)_{18}$ and $(C_{12}H_{25}Se)_2$ (Figures 8(b) and S17). The reaction of $Au_n(SR)_m$ clusters with diselenide is often used for the synthesis of $Au_n(SeR)_m$ clusters,[56,57] but little is known about its mechanism. As shown in Figure 8(b), $Au_{24}Pd(SC_2H_4Ph)_{18-n}(SeC_{12}H_{25})_n$ (n = 1, 2) clusters have

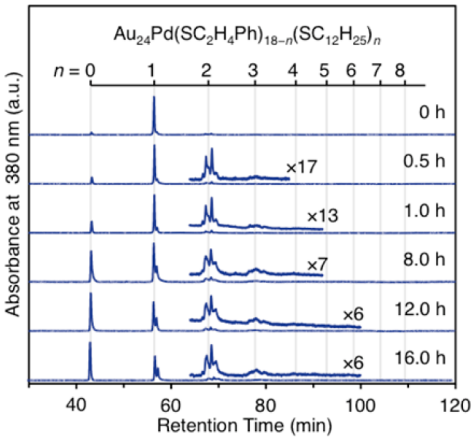

Figure 9. Time dependence of chromatogram of core-site type $Au_{24}Pd(SC_2H_4Ph)_{17}(SC_{12}H_{25})$ left in acetone.

slightly longer retention times compared with $Au_{24}Pd(SC_2H_4Ph)_{18-n}(SC_{12}H_{25})_n$ (n = 1, 2) (Figures 4(c) and 8(a)) probably because of the difference in atomic radius between Se (1.17 Å) and S (1.04 Å) (Figure S18). However, chromatograms of the respective clusters are essentially similar (Figure S18). This means that the exchange reaction occurs preferentially at a core site even if the introduced ligand is selenolate instead of thiolate (Figure S19). These results demonstrate that the priority of the reaction site does not change in all the aforementioned reactions on $Au_{24}Pd(SC_2H_4Ph)_{18}$.

Mechanism of the Variation in Isomer Distributions. We further studied on how isomer distributions arise in clusters in solution (Figure 6) by tracking the temporal evolution of a chromatogram of isomer-separated $Au_{24}Pd(SC_2H_4Ph)_{17}(SC_{12}H_{25})$ by RP-HPLC. Figure 9 shows this evolution for a core-site isomer. During the first hour, the amount of $Au_{24}Pd(SC_2H_4Ph)_{17}(SC_{12}H_{25})$ decreased gradually, whereas the amounts of $Au_{24}Pd(SC_2H_4Ph)_{18}$ and $Au_{24}Pd(SC_2H_4Ph)_{16}(SC_{12}H_{25})_2$ increased gradually. At this stage, the isomer distribution of $Au_{24}Pd(SC_2H_4Ph)_{17}(SC_{12}H_{25})$ did not display noticeable changes. This means that the main reaction in this time frame is the ligand-exchange reaction between $Au_{24}Pd(SC_2H_4Ph)_{17}(SC_{12}H_{25})$ shown in Scheme 1(a).[53] The reaction in Scheme 1(a) had progressed even further (Figure 9) after an extended period (≥8 h). A sample of this time frame includes $Au_{24}Pd(SC_2H_4Ph)_{18}$ and $Au_{24}Pd(SC_2H_4Ph)_{16}(SC_{12}H_{25})_2$ produced by the reaction in Scheme 1(a) in relatively large quantities and $Au_{24}Pd(SC_2H_4Ph)_{18-n}(SC_{12}H_{25})_n$ ($n \geq 3$) produced by the multiple ligand-exchange reactions between clusters in small quantities (Figure 9). In these samples, the ligand-exchange reaction depicted in Scheme 1(b,c) can be expected to occur frequently between the generated clusters. Accordingly, a considerable degree of apex-site isomer started to appear in the region of $Au_{24}Pd(SC_2H_4Ph)_{17}(SC_{12}H_{25})$ in addition to the core-site isomer in the chromatograms of such timeframes. Similar phenomena were also

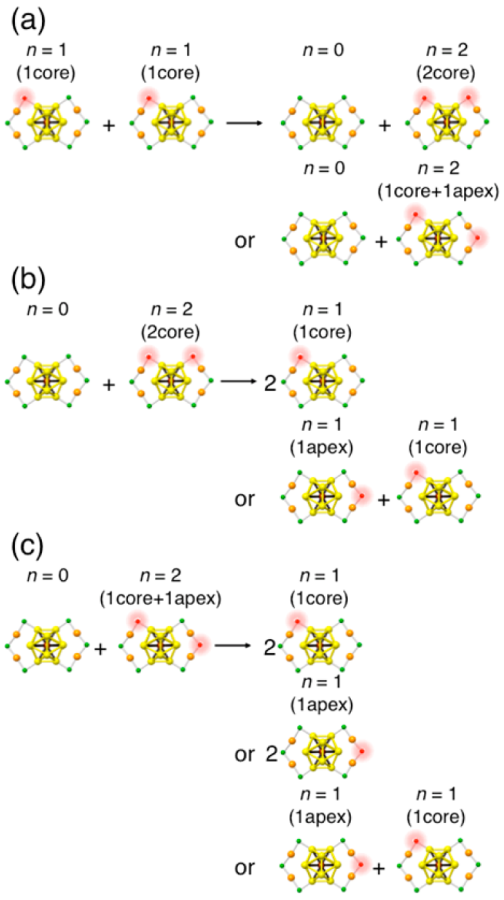

Scheme 1. Proposed reactions that could lead to the production of apex-site type $Au_{24}Pd(SC_2H_4Ph)_{17}(SC_{12}H_{25})$ from core-site type $Au_{24}Pd(SC_2H_4Ph)_{17}(SC_{12}H_{25})$. Each isomer structure is schematic and is not the exact structure that was determined experimentally for the clusters included in the solution.

observed in the experiment using $Au_{24}Pd(SC_2H_4Ph)_{17}(SC_{12}H_{25})$ of apex-site isomer, although the generation rate of isomer distribution is slightly different (Figure S20). These results imply that the variation in isomer distribution in $Au_{24}Pd(SC_2H_4Ph)_{17}(SC_{12}H_{25})$ is caused mainly by the ligand-exchange reactions between the generated clusters.

Isomer Distribution in $Au_{24}Pd(SC_2H_4Ph)_{16}(SC_{12}H_{25})_2$ Generated from Isomer-Separated $Au_{24}Pd(SC_2H_4Ph)_{17}(SC_{12}H_{25})$. Our study on the temporal evolution of isomer-separated $Au_{24}Pd(SC_2H_4Ph)_{17}(SC_{12}H_{25})$ using RP-HPLC also revealed that the isomer distribution of $Au_{24}Pd(SC_2H_4Ph)_{16}(SC_{12}H_{25})_2$ generated by $Au_{24}Pd(SC_2H_4Ph)_{17}(SC_{12}H_{25})$ is different depending on the isomer structure of the precursor $Au_{24}Pd(SC_2H_4Ph)_{17}(SC_{12}H_{25})$. Figure 10 shows chromatograms of $Au_{24}Pd(SC_2H_4Ph)_{16}(SC_{12}H_{25})_2$ generated after 0.5 h (Figures 9 and S20). The chromatogram of $Au_{24}Pd(SC_2H_4Ph)_{16}(SC_{12}H_{25})_2$ generated from a core-site isomer (Figure 10(b)) resembles closely that of $Au_{24}Pd(SC_2H_4Ph)_{16}(SC_{12}H_{25})_2$ obtained by ligand-exchange reaction between $Au_{24}Pd(SC_2H_4Ph)_{18}$ and $C_{12}H_{25}SH$ (Figures 4(c) and 10(a)), supporting the interpretation that the exchange

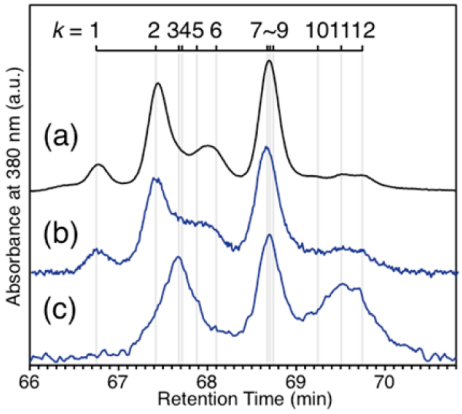

Figure 10. Chromatograms of the region of $Au_{24}Pd(SC_2H_4Ph)_{16}(SC_{12}H_{25})_2$ obtained by (a) reaction between $Au_{24}Pd(SC_2H_4Ph)_{18}$ and $C_{12}H_{25}SH$ in dichloromethane (Figure 4(c)), (b) standing of core-site type $Au_{24}Pd(SC_2H_4Ph)_{17}(SC_{12}H_{25})$ in acetone (Figure 9), and (c) standing of apex-site type $Au_{24}Pd(SC_2H_4Ph)_{17}(SC_{12}H_{25})$ in acetone (Figure S20). Index *k* indicates the isomer index used for tentative assignment of each isomer in Figure S11 (Table S3).

occurs preferentially at a core site in the reaction between $Au_{24}Pd(SC_2H_4Ph)_{18}$ and $C_{12}H_{25}SH$. Conversely, $Au_{24}Pd(SC_2H_4Ph)_{16}(SC_{12}H_{25})_2$ generated from an apex-site isomer (Figure S20) exhibited strong peaks at different retention times (Figure 10(c)). These observed peaks were located mainly at the retention times predicted for $Au_{24}Pd(SC_2H_4Ph)_{16}(SC_{12}H_{25})_2$ including exchange at the apex site (Figures S12 and S21). Our tentative assignments of the peaks of $Au_{24}Pd(SC_2H_4Ph)_{16}(SC_{12}H_{25})_2$ imply that the sample in Figure 10(b) contains isomers with two $SC_{12}H_{25}$ at the core sites (isomer index j = 1−5) with a content of 71.6% as main product (Figure S21), whereas the sample of Figure 10(c) contains isomers with one $SC_{12}H_{25}$ at the core site and one $SC_{12}H_{25}$ at the apex site (isomer index j = 6−10) with content of 78.3% as main product (Figure S21). These results demonstrate that the isomer distribution of the generated clusters is different. A similar phenomenon was also observed for $Au_{24}Pd(SC_2H_4Ph)_{15}(SC_{12}H_{25})_3$ (Figure S22). These results indicate that the coordination isomer distribution of the products generated by the ligand-exchange reactions between clusters could be controlled by controlling the coordination isomer distribution of the reactant clusters.

CONCLUSIONS

We have evaluated quantitatively the isomer distribution of the product obtained by a ligand-exchange reaction on $Au_{24}Pd(SC_2H_4Ph)_{18}$ by increasing the RP-HPLC resolution. The following were concluded concerning the mechanism of ligand-exchange reactions on the clusters. (i) The exchange reactions occur preferentially at thiolates of a core site in the ligand-exchange reactions of $Au_{24}Pd(SC_2H_4Ph)_{18}$ with all molecules of RSH (R = C_xH_{2x+1}; x = 8, 10, 12, or 14),

$(C_{12}H_{25}S)_2$, or $(C_{12}H_{25}Se)_2$. (ii) The ligand-exchange reactions between clusters occur in the cluster solution, and this causes a variation in coordination isomer distribution of the clusters in solution. (iii) The control of coordination isomer distribution of the reactant clusters enables control of the coordination isomer distribution of the product generated by ligand-exchange reactions between clusters. We used $Au_{24}Pd(SC_2H_4Ph)_{18}$ in this study as a model cluster to accurately determine the isomer distribution of the products. However, $Au_{24}Pd(SC_2H_4Ph)_{18}$ has a similar framework structure to $Au_{25}(SR)_{18}$ (Figure 1(a,b)). Therefore, the results obtained are expected to be applicable for ligand-exchange reactions on $Au_{25}(SR)_{18}$ and other $Au_n(SR)_m$ clusters. We believe that observing and understanding such reactions could lead to their improved control and thereby the creation of desired metal clusters.

METHODS

Synthesis of $Au_{24}Pd(SC_2H_4Ph)_{18}$. $Au_{24}Pd(SC_{12}H_{25})_{18}$ was first synthesized by a method previously reported by our group[43] which is based on the Brust method.[58] Then, all $Au_{24}Pd(SC_{12}H_{25})_{18}$ ligands were replaced with SC_2H_4Ph by reacting $Au_{24}Pd(SC_{12}H_{25})_{18}$ with PhC_2H_4SH in dichloromethane. We repeated two procedures several times to achieve this: a ligand-exchange reaction and washing of excess PhC_2H_4SH and byproducts from the products using a 1:1 water:methanol solution. The $Au_{24}Pd(SC_2H_4Ph)_{18}$ was obtained with molecular purity (Figure S1).

Ligand-Exchange Reaction. $Au_{24}Pd(SC_2H_4Ph)_{18}$ (0.10 μmol) was dissolved in 100 μL of dichloromethane, toluene, or acetone. To this solution, 5.0 μmol of RSH ($R = C_xH_{2x+1}$; $x = 8$, 10, 12, or 14), 5.0 μmol of $(C_{12}H_{25}S)_2$, or 1.0 μmol of $(C_{12}H_{25}Se)_2$ was added and the solution was stirred at room temperature. $(C_{12}H_{25}S)_2$ and $(C_{12}H_{25}Se)_2$ were synthesized using the methods of Tong and co-workers.[59,60] After 4 min ($C_xH_{2x+1}RH$), 1 h ($(C_{12}H_{25}S)_2$), or 40 s ($(C_{12}H_{25}Se)_2$), the solution was washed with a mixture of methanol and water to remove excess thiols.

Temporal Evolution of Isomer-Separated $Au_{24}Pd(SC_2H_4Ph)_{17}(SC_{12}H_{25})$. Each coordination isomer (core- or apex-site isomer) of $Au_{24}Pd(SC_2H_4Ph)_{17}(SC_{12}H_{25})$ was separated using RP-HPLC (Figure 6(a)). The separated sample (~8 nmol) was left in 50 μL of acetone, and the product temporal evolution was evaluated by RP-HPLC.

Characterization. MALDI mass spectra were acquired with a time-of-flight mass spectrometer (JEOL Ltd., JMS-S3000) using an Nd:YAG laser (wavelength: 349 nm) and *trans*-2-[3-(4-*tert*-butylphenyl)-2-methyl-2-propenylidene]malononitrile as the MALDI matrix.[36] The cluster-to-matrix ratio was set at 1:1000. The laser fluence was reduced to the lowest value that enabled ion detection. Ultraviolet−visible/near-infrared absorption spectra of the $Au_{24}Pd(SC_2H_4Ph)_{18}$ dichloromethane solution were recorded at ambient temperature using a spectrometer (JASCO, V-670). Wavelength-dependent optical data, $I(w)$, were converted to energy-dependent data, $I(E)$, using the following relation, such that the integrated spectral areas were conserved: $I(E) = I(w)/|\partial E/\partial w| \propto I(w) \times w^2$.

HPLC Experiments. HPLC experiments were conducted using a Shimadzu instrument consisting of a DGU-20A3R online degasser, LC-20AD pump, CTO-20AC column oven, and SPD-M20A photodiode array detector. A stainless-steel column (250 mm × 4.6 mm inner diameter) packed with 5 μm C18-bonded silica with a pore size of 175 Å (Hypersil GOLD, Thermo Scientific) was used as the reverse-phase column. The column temperature was fixed at 25 °C to maintain reproducibility. Before sample injection, aging (stabilization) of the column and detector was performed for a sufficient time. The absorbance chromatogram was monitored, using a photodiode array, at 380 nm. Each sample was first diluted in acetone (0.1 mg/5 μL) and then suspended in solution by adding acetonitrile (15 μL). The sample suspension (20 μL) was injected into the instrument with an acetonitrile mobile phase at 1 mL/min. After sample injection, the amount of acetone in the mobile phase was increased continuously, using a linear gradient program that increased the acetone ratio of the mobile phase from 0 to 100%, with a replacement time of 100 min (Figure S4). In a previous study, the use of a step gradient as a gradient program improved the resolution.[46] However, a clear improvement in resolution was not observed for the experimental conditions used. After analysis, the chromatogram was corrected by subtracting the background measured without a sample.

Conflict of Interest: The authors declare no competing financial interest.

Acknowledgment. We thank M. Yamaguchi and C. Uchida for technical assistance and W. Kurashige for his valuable comments. This work was supported by a Grant-in-Aid for Scientific Research on Innovative Areas "New Polymeric Materials Based on Element-Blocks (No. 2401)" (15H00763) of The Ministry of Education, Culture, Sports, Science, and Technology, Japan, the Canon Foundation, the Kajima Foundation, and the Nippon Sheet Foundation for Materials Science and Engineering. The first author expresses his gratitude to the Sasagawa Foundation for partial financial support.

Supporting Information Available: The counting method for the number of repetitions of site combinations for each isomer of $Au_{24}Pd(SC_2H_4Ph)_{18-n}(SC_{12}H_{25})_n$ ($n = 1$, 2), various solvent properties, and additional product characterization. The Supporting Information is available free of charge on the ACS Publications website at DOI: 10.1021/acsnano.5b03435.

REFERENCES AND NOTES

1. Tsukuda, T. Toward an Atomic-Level Understanding of Size-Specific Properties of Protected and Stabilized Gold Clusters. *Bull. Chem. Soc. Jpn.* **2012**, *85*, 151–168.
2. Whetten, R. L.; Khoury, J. T.; Alvarez, M. M.; Murthy, S.; Vezmar, I.; Wang, Z. L.; Stephens, P. W.; Cleveland, C. L.; Luedtke, W. D.; Landman, U. Nanocrystal Gold Molecules. *Adv. Mater.* **1996**, *8*, 428–433.
3. Parker, J. F.; Fields-Zinna, C. A.; Murray, R. W. The Story of a Monodisperse Gold Nanoparticle: $Au_{25}L_{18}$. *Acc. Chem. Res.* **2010**, *43*, 1289–1296.
4. Walter, M.; Akola, J.; Lopez-Acevedo, O.; Jadzinsky, P. D.; Calero, G.; Ackerson, C. J.; Whetten, R. L.; Grönbeck, H.; Häkkinen, H. A Unified View of Ligand−Protected Gold Clusters as Superatom Complexes. *Proc. Natl. Acad. Sci. U. S. A.* **2008**, *105*, 9157–9162.
5. Negishi, Y.; Nobusada, K.; Tsukuda, T. Glutathione-Protected Gold Clusters Revisited: Bridging the Gap between Gold(I)-Thiolate Complexes and Thiolate-Protected Gold Nanocrystals. *J. Am. Chem. Soc.* **2005**, *127*, 5261–5270.
6. Qian, H.; Zhu, M.; Wu, Z.; Jin, R. Quantum Sized Gold Nanoclusters with Atomic Precision. *Acc. Chem. Res.* **2012**, *45*, 1470–1479.
7. Dharmaratne, A. C.; Krick, T.; Dass, A. Nanocluster Size Evolution Studied by Mass Spectrometry in Room Temperature $Au_{25}(SR)_{18}$ Synthesis. *J. Am. Chem. Soc.* **2009**, *131*, 13604–13605.
8. Luo, Z.; Nachammai, V.; Zhang, B.; Yan, N.; Leong, D. T.; Jiang, D.-e.; Xie, J. Toward Understanding the Growth Mechanism: Tracing All Stable Intermediate Species from Reduction of Au(I)−Thiolate Complexes to Evolution of Au_{25} Nanoclusters. *J. Am. Chem. Soc.* **2014**, *136*, 10577–10580.

9. Dainese, T.; Antonello, S.; Gascón, J. A.; Pan, F.; Perera, N. V.; Ruzzi, M.; Venzo, A.; Zoleo, A.; Rissanen, K.; Maran, F. $Au_{25}(SEt)_{18}$, a Nearly Naked Thiolate-Protected Au_{25} Cluster: Structural Analysis by Single Crystal X-ray Crystallography and Electron Nuclear Double Resonance. *ACS Nano* **2014**, *8*, 3904–3912.
10. Wang, S.; Song, Y.; Jin, S.; Liu, X.; Zhang, J.; Pei, Y.; Meng, X.; Chen, M.; Li, P.; Zhu, M. Metal Exchange Method Using Au_{25} Nanoclusters as Templates for Alloy Nanoclusters with Atomic Precision. *J. Am. Chem. Soc.* **2015**, *137*, 4018–4021.
11. Negishi, Y.; Nakazaki, T.; Malola, S.; Takano, S.; Niihori, Y.; Kurashige, W.; Yamazoe, S.; Tsukuda, T.; Häkkinen, H. A Critical Size for Emergence of Nonbulk Electronic and Geometric Structures in Dodecanethiolate-Protected Au Clusters. *J. Am. Chem. Soc.* **2015**, *137*, 1206–1212.
12. Dolamic, I.; Knoppe, S.; Dass, A.; Bürgi, T. First Enantioseparation and Circular Dichroism Spectra of Au_{38} Clusters Protected by Achiral Ligands. *Nat. Commun.* **2012**, *3*, 798–803.
13. Malola, S.; Lehtovaara, L.; Enkovaara, J.; Häkkinen, H. Birth of the Localized Surface Plasmon Resonance in Monolayer-Protected Gold Nanoclusters. *ACS Nano* **2013**, *7*, 10263–10270.
14. Jiang, D.-e.; Kühn, M.; Tang, Q.; Weigend, F. Superatomic Orbitals under Spin-Orbit Coupling. *J. Phys. Chem. Lett.* **2014**, *5*, 3286–3289.
15. Fernando, A.; Weerawardene, K. L. D. M.; Karimova, N. V.; Aikens, C. M. Quantum Mechanical Studies of Large Metal, Metal Oxide, and Metal Chalcogenide Nanoparticles and Clusters. *Chem. Rev.* **2015**, *115*, 6112–6216.
16. Liu, C.; Lin, S.; Pei, Y.; Zeng, X. C. Semiring Chemistry of $Au_{25}(SR)_{18}$: Fragmentation Pathway and Catalytic Active Site. *J. Am. Chem. Soc.* **2013**, *135*, 18067–18079.
17. Tlahuice-Flores, A. New Insight into the Structure of Thiolated Gold Clusters: A Structural Prediction of the $Au_{187}(SR)_{68}$ Cluster. *Phys. Chem. Chem. Phys.* **2015**, *17*, 5551–5555.
18. Devadas, M. S.; Bairu, S.; Qian, H.; Sinn, E.; Jin, R.; Ramakrishna, G. Temperature-Dependent Optical Absorption Properties of Monolayer-Protected Au_{25} and Au_{38} Clusters. *J. Phys. Chem. Lett.* **2011**, *2*, 2752–2758.
19. Bigioni, T. P.; Whetten, R. L.; Dag, Ö. Near-Infrared Luminescence from Small Gold Nanocrystals. *J. Phys. Chem. B* **2000**, *104*, 6983–6986.
20. Ramakrishna, G.; Varnavski, O.; Kim, J.; Lee, D.; Goodson, T. Quantum-Sized Gold Clusters as Efficient Two-Photon Absorbers. *J. Am. Chem. Soc.* **2008**, *130*, 5032–5033.
21. Kwak, K.; Kumar, S. S.; Pyo, K.; Lee, D. Ionic Liquid of a Gold Nanocluster: A Versatile Matrix for Electrochemical Biosensors. *ACS Nano* **2014**, *8*, 671–679.
22. Li, G.; Jin, R. Atomically Precise Gold Nanoclusters as New Model Catalysts. *Acc. Chem. Res.* **2013**, *46*, 1749–1758.
23. Kauffman, D. R.; Alfonso, D.; Matranga, C.; Qian, H.; Jin, R. Experimental and Computational Investigation of Au_{25} Clusters and CO_2: A Unique Interaction and Enhanced Electrocatalytic Activity. *J. Am. Chem. Soc.* **2012**, *134*, 10237–10243.
24. Wu, Z.; Jiang, D.-e.; Mann, A. K. P.; Mullins, D. R.; Qiao, Z.-A.; Allard, L. F.; Zeng, C.; Jin, R.; Overbury, S. H. Thiolate Ligands as a Double-Edged Sword for CO Oxidation on CeO_2 Supported $Au_{25}(SCH_2CH_2Ph)_{18}$ Nanoclusters. *J. Am. Chem. Soc.* **2014**, *136*, 6111–6122.
25. Huang, P.; Chen, G.; Jiang, Z.; Jin, R.; Zhu, Y.; Sun, Y. Atomically Precise Au_{25} Superatoms Immobilized on CeO_2 Nanorods for Styrene Oxidation. *Nanoscale* **2013**, *5*, 3668–3672.
26. Nie, X.; Zeng, C.; Ma, X.; Qian, H.; Ge, Q.; Xu, H.; Jin, R. CeO_2-Supported $Au_{38}(SR)_{24}$ Nanocluster Catalysts for CO Oxidation: A Comparison of Ligand-on and -off Catalysts. *Nanoscale* **2013**, *5*, 5912–5918.
27. Shibu, E. S.; Muhammed, M. A. H.; Tsukuda, T.; Pradeep, T. Ligand Exchange of $Au_{25}SG_{18}$ Leading to Functionalized Gold Clusters: Spectroscopy, Kinetics, and Luminescence. *J. Phys. Chem. C* **2008**, *112*, 12168–12176.
28. Holm, A. H.; Ceccato, M.; Donkers, R. L.; Fabris, L.; Pace, G.; Maran, F. Effect of Peptide Ligand Dipole Moments on the Redox Potentials of Au_{38} and Au_{140} Nanoparticles. *Langmuir* **2006**, *22*, 10584–10589.
29. Zeng, C.; Qian, H.; Li, T.; Li, G.; Rosi, N. L.; Yoon, B.; Barnett, R. N.; Whetten, R. L.; Landman, U.; Jin, R. Total Structure and Electronic Properties of the Gold Nanocrystal $Au_{36}(SR)_{24}$. *Angew. Chem., Int. Ed.* **2012**, *51*, 13114–13118.
30. Zeng, C.; Liu, C.; Pei, Y.; Jin, R. Thiol Ligand-Induced Transformation of $Au_{38}(SC_2H_4Ph)_{24}$ to $Au_{36}(SPh\text{-}t\text{-}Bu)_{24}$. *ACS Nano* **2013**, *7*, 6138–6145.
31. Zeng, C.; Li, T.; Das, A.; Rosi, N. L.; Jin, R. Chiral Structure of Thiolate-Protected 28-Gold-Atom Nanocluster Determined by X-ray Crystallography. *J. Am. Chem. Soc.* **2013**, *135*, 10011–10013.
32. Nimmala, P. R.; Theivendran, S.; Barcaro, G.; Sementa, L.; Kumara, C.; Jupally, V. R.; Apra, E.; Stener, M.; Fortunelli, A.; Dass, A. Transformation of $Au_{144}(SCH_2CH_2Ph)_{60}$ to $Au_{133}(SPh\text{-}t\text{Bu})_{52}$ Nanomolecules: Theoretical and Experimental Study. *J. Phys. Chem. Lett.* **2015**, *6*, 2134–2139.
33. Zeng, C.; Chen, Y.; Kirschbaum, K.; Appavoo, K.; Sfeir, M. Y.; Jin, R. Structural Patterns at All Scales in a Nonmetallic Chiral $Au_{133}(SR)_{52}$ Nanoparticle. *Sci. Adv.* **2015**, *1*, e1500045.
34. Guo, R.; Song, Y.; Wang, G.; Murray, R. W. Does Core Size Matter in the Kinetics of Ligand Exchanges of Monolayer-Protected Au Clusters? *J. Am. Chem. Soc.* **2005**, *127*, 2752–2757.
35. Tracy, J. B.; Crowe, M. C.; Parker, J. F.; Hampe, O.; Fields-Zinna, C. A.; Dass, A.; Murray, R. W. Electrospray Ionization Mass Spectrometry of Uniform and Mixed Monolayer Nanoparticles: $Au_{25}[S(CH_2)_2Ph]_{18}$ and $Au_{25}[S(CH_2)_2Ph]_{18\text{-}x}(SR)_x$. *J. Am. Chem. Soc.* **2007**, *129*, 16209–16215.
36. Dass, A.; Stevenson, A.; Dubay, G. R.; Tracy, J. B.; Murray, R. W. Nanoparticle MALDI-TOF Mass Spectrometry without Fragmentation: $Au_{25}(SCH_2CH_2Ph)_{18}$ and Mixed Monolayer $Au_{25}(SCH_2CH_2Ph)_{18\text{-}x}(L)_x$. *J. Am. Chem. Soc.* **2008**, *130*, 5940–5946.
37. Hostetler, M. J.; Templeton, A. C.; Murray, R. W. Dynamics of Place-Exchange Reactions on Monolayer-Protected Gold Cluster Molecules. *Langmuir* **1999**, *15*, 3782–3789.
38. Heinecke, C. L.; Ni, T. W.; Malola, S.; Mäkinen, V.; Wong, O. A.; Häkkinen, H.; Ackerson, C. J. Structural and Theoretical Basis for Ligand Exchange on Thiolate Monolayer Protected Gold Nanoclusters. *J. Am. Chem. Soc.* **2012**, *134*, 13316–13322.
39. Ni, T. W.; Tofanelli, M. A.; Phillips, B. D.; Ackerson, C. J. Structural Basis for Ligand Exchange on $Au_{25}(SR)_{18}$. *Inorg. Chem.* **2014**, *53*, 6500–6502.
40. Beqa, L.; Deschamps, D.; Perrio, S.; Gaumont, A.-C.; Knoppe, S.; Bürgi, T. Ligand Exchange Reaction on $Au_{38}(SR)_{24}$, Separation of $Au_{38}(SR)_{23}(SR')_1$ Regioisomers, and Migration of Thiolates. *J. Phys. Chem. C* **2013**, *117*, 21619–21625.
41. Wolfe, R. L.; Murray, R. W. Analytical Evidence for the Monolayer-Protected Cluster $Au_{225}[(S(CH_2)_5CH_3)]_{75}$. *Anal. Chem.* **2006**, *78*, 1167–1173.
42. Choi, M. M. F.; Douglas, A. D.; Murray, R. W. Ion-Pair Chromatographic Separation of Water-Soluble Gold Monolayer-Protected Clusters. *Anal. Chem.* **2006**, *78*, 2779–2785.
43. Negishi, Y.; Kurashige, W.; Niihori, Y.; Iwasa, T.; Nobusada, K. Isolation, Structure, and Stability of a Dodecanethiolate-Protected Pd_1Au_{24} Cluster. *Phys. Chem. Chem. Phys.* **2010**, *12*, 6219–6225.
44. Negishi, Y.; Sakamoto, C.; Ohyama, T.; Tsukuda, T. Synthesis and the Origin of the Stability of Thiolate-Protected Au_{130} and Au_{187} Clusters. *J. Phys. Chem. Lett.* **2012**, *3*, 1624–1628.
45. Niihori, Y.; Matsuzaki, M.; Pradeep, T.; Negishi, Y. Separation of Precise Compositions of Noble Metal Clusters Protected with Mixed Ligands. *J. Am. Chem. Soc.* **2013**, *135*, 4946–4949.
46. Niihori, Y.; Matsuzaki, M.; Uchida, C.; Negishi, Y. Advanced Use of High-Performance Liquid Chromatography for Synthesis of Controlled Metal Clusters. *Nanoscale* **2014**, *6*, 7889–7896.

47. Negishi, Y.; Kurashige, W.; Niihori, Y.; Nobusada, K. Toward the Creation of Stable, Functionalized Metal Clusters. *Phys. Chem. Chem. Phys.* **2013**, *15*, 18736–18751.
48. Negishi, Y.; Kurashige, K.; Kobayashi, Y.; Yamazoe, Y.; Kojima, N.; Seto, M.; Tsukuda, T. Formation of a Pd@Au_{12} Superatomic Core in $Au_{24}Pd_1(SC_{12}H_{25})_{18}$ Probed by ^{197}Au Mössbauer and Pd K-Edge EXAFS Spectroscopy. *J. Phys. Chem. Lett.* **2013**, *4*, 3579–3583.
49. Kurashige, W.; Niihori, Y.; Sharma, S.; Negishi, Y. Recent Progress in the Functionalization Methods of Thiolate-Protected Gold Clusters. *J. Phys. Chem. Lett.* **2014**, *5*, 4134–4142.
50. Heaven, M. W.; Dass, A.; White, P. S.; Holt, K. M.; Murray, R. W. Crystal Structure of the Gold Nanoparticle $[N(C_8H_{17})_4][Au_{25}(SCH_2CH_2Ph)_{18}]$. *J. Am. Chem. Soc.* **2008**, *130*, 3754–3755.
51. Zhu, M.; Aikens, C. M.; Hollander, F. J.; Schatz, G. C.; Jin, R. Correlating the Crystal Structure of A Thiol-Protected Au_{25} Cluster and Optical Properties. *J. Am. Chem. Soc.* **2008**, *130*, 5883–5885.
52. Akola, J.; Walter, M.; Whetten, R. L.; Häkkinen, H.; Grönbeck, H. On the Structure of Thiolate-Protected Au_{25}. *J. Am. Chem. Soc.* **2008**, *130*, 3756–3757.
53. Niihori, Y.; Kurashige, W.; Matsuzaki, M.; Negishi, Y. Remarkable Enhancement in Ligand-Exchange Reactivity of Thiolate-Protected Au_{25} Nanoclusters by Single Pd Atom Doping. *Nanoscale* **2013**, *5*, 508–512.
54. Lide, D. R. *CRC Handbook of Chemistry and Physics*, 89th ed.; CRC Press: New York, 2008; 6-p197.
55. Horváth, C. *High-Performance Liquid Chromatography: Advances and Perspectives*; Academic Press: New York, 1980; Vol. 2, p 167.
56. Meng, X.; Xu, Q.; Wang, S.; Zhu, M. Ligand-Exchange Synthesis of Selenophenolate-Capped Au_{25} Nanoclusters. *Nanoscale* **2012**, *4*, 4161–4165.
57. Kurashige, W.; Yamazoe, S.; Kanehira, K.; Tsukuda, T.; Negishi, Y. Selenolate-Protected Au_{38} Nanoclusters: Isolation and Structural Characterization. *J. Phys. Chem. Lett.* **2013**, *4*, 3181–3185.
58. Brust, M.; Walker, M.; Bethell, D.; Schiffrin, D. J.; Whyman, R. Synthesis of Thiol-Derivatized Gold Nanoparticles in a Two-Phase Liquid–Liquid System. *J. Chem. Soc., Chem. Commun.* **1994**, *7*, 801–802.
59. Li, Y.; Zaluzhna, O.; Xu, B.; Gao, Y.; Modest, J. M.; Tong, Y. Y. J. Mechanistic Insights into the Brust-Schiffrin Two-Phase Synthesis of Organo-chalcogenate-Protected Metal Nanoparticles. *J. Am. Chem. Soc.* **2011**, *133*, 2092–2095.
60. Deacon, M. L.; Zelakiewicz, B. S.; Tong, Y. Y. A Fast and Convenient One-Pot Synthesis of Dioctyldiselenide at Ambient Temperature and Atmosphere. *Synlett* **2005**, *2005*, 1618–1620.